

## High-entropy Ti-Zr-Nb-Hf-Ta carbide and carbonitride coatings fabricated by high-speed arc discharge plasma jet

Dmitry S. Nikitin <sup>a</sup>, Ivan I. Shanenkov <sup>a,\*</sup>, Artur Nassyrbayev <sup>a</sup>, Alexander A. Sivkov <sup>a</sup>, Viktor S. Baidyshev <sup>b</sup>, Yulia A. Kvashnina <sup>c</sup>, Nikita A. Matsokin <sup>b</sup>, Alexander Ya. Pak <sup>a</sup>, Alexander G. Kvashnin <sup>b,\*\*</sup>

<sup>a</sup> National Research Tomsk Polytechnic University, 30 Lenin Avenue, Tomsk 634050, Russia

<sup>b</sup> Skolkovo Institute of Science and Technology, Skolkovo Innovation Center, Bolshoy Boulevard 30, bld. 1, Moscow 121205, Russia

<sup>c</sup> Pirogov Russian National Research Medical University, 1 Ostrovityanova St., Moscow, Russia

### ARTICLE INFO

#### Keywords:

High-entropy carbides  
High-entropy carbonitrides  
Coatings  
Plasma spraying  
Computational discovery

### ABSTRACT

The interest in high-entropy materials is constantly growing since their predicted properties can help to overcome current limitations in different application areas. Despite the number of modeled and calculated high-entropy compounds, there is still a problem with their effective synthesis in the forms of bulk products and coatings, which prevents unambiguous determination of their predicted properties. We develop and demonstrate a new method for preparing high-entropy carbide and carbonitride coatings of IV-V transition metal compounds, using  $(\text{TiZrNbHfTa})_{\text{x}}\text{C}_{\text{y}}$  as an example. The developed technique based on the application of a high-speed arc discharge plasma jet leads to the synthesis of a high-entropy carbide  $\text{TiZrNbHfTaC}_5$  coating and corresponding carbonitride coatings with a thickness of up to 20  $\mu\text{m}$ . The results of studying the physical and mechanical properties of synthesized high-entropy coatings generally confirm the predictions of the preliminary modeling in terms of mechanical properties. Although they are superior in hardness ( $\sim 32 \text{ GPa}$  vs.  $25 \text{ GPa}$ ). In combination with high oxidation resistance (up to  $700^\circ\text{C}$ ), this indicates the possibility of applying such materials not only to creating heat-resistant products, but also significantly strengthening them. The implications and significance of this work extend far beyond the results shown here, as it opens the door to synthesizing many functional high-entropy coatings with different compositions to investigate their properties and performance.

### 1. Introduction

Today, the aerospace industry continues to rapidly develop, while demands for the durability, reliability, and longevity of the structures used are simultaneously increasing. In this regard, the development of new classes of materials for the aerospace industry is of particular interest, as the thermal and mechanical performance limits of known compounds have been reached. In an attempt to overcome the existing limitations, scientists paid their attention to materials of the ultra-high temperature ceramics (UHTCs) class, since they can be applied in harsh operating conditions [1–3]. Studies of binary transition metal carbides, such as HfC, ZrC, and TiC, possessing high melting points

( $>3000^\circ\text{C}$ ), high modulus, high hardness, and excellent oxidation resistance [4,5], gave a ground to expand the number of UHTCs materials but not to overcome the operating restrictions. In this regard, the development of multi-component materials for the UTHCs applications is still urgent and practically important. Machine learning techniques can help solve this problem because they have made it possible to predict new promising structures and compounds, model their potential properties, and subsequently synthesize them by chemical or physical methods [6,7].

In the field of multicomponent UHTCs, high-entropy materials (HEM) have recently been paid extensive attention due to their unique and intriguing properties. New field of materials science related to high-

\* Correspondence to: I.I. Shanenkov, School of Energy and Power Engineering, National Research Tomsk Polytechnic University, 30 Lenin Avenue, Tomsk 634050, Russian Federation.

\*\* Correspondence to: A.G. Kvashnin, Skolkovo Institute of Science and Technology, Skolkovo Innovation Center, Bolshoy Boulevard 30, bld. 1, Moscow 121205, Russian Federation.

E-mail addresses: [nikitindmsr@tpu.ru](mailto:nikitindmsr@tpu.ru) (D.S. Nikitin), [shanenkovii@tpu.ru](mailto:shanenkovii@tpu.ru) (I.I. Shanenkov), [arn1@tpu.ru](mailto:arn1@tpu.ru) (A. Nassyrbayev), [sivkov@tpu.ru](mailto:sivkov@tpu.ru) (A.A. Sivkov), [V.Baidyshev@skoltech.ru](mailto:V.Baidyshev@skoltech.ru) (V.S. Baidyshev), [N.Matsokin@skoltech.ru](mailto:N.Matsokin@skoltech.ru) (N.A. Matsokin), [ayapak@tpu.ru](mailto:ayapak@tpu.ru) (A.Ya. Pak), [A.Kvashnin@skoltech.ru](mailto:A.Kvashnin@skoltech.ru) (A.G. Kvashnin).

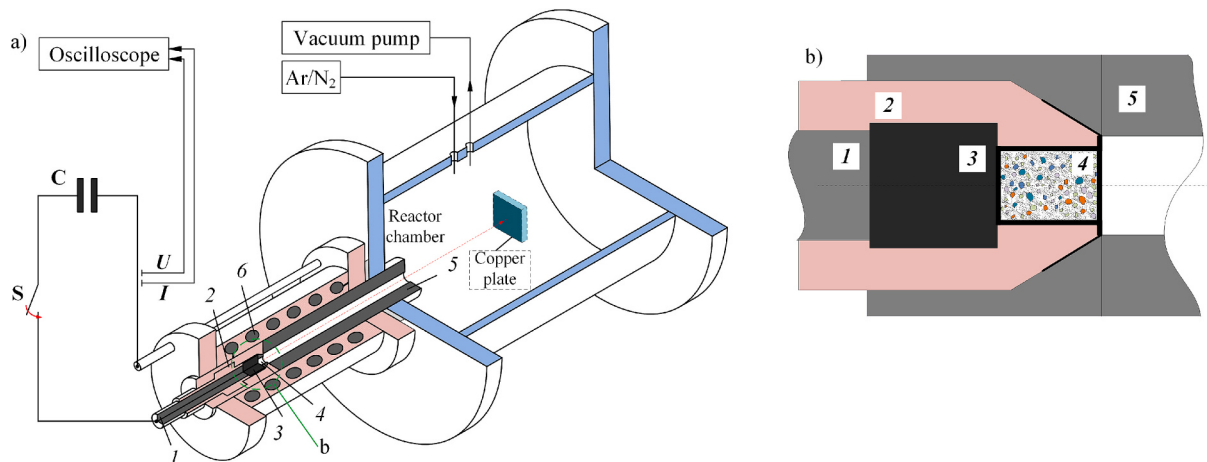


**Fig. 1.** Scheme of the experimental setup (a) and the main node of the plasma formation (b): 1 – central electrode, 2 – central electrode insulator, 3 – graphite insert of the central electrode, 4 – plasma formation zone with metal precursors, 5 – graphite accelerating channel of the barrel electrode, 6 – inductor.

entropy compounds started from the comprehensive studies of high-entropy alloys (HEA) [8,9]. Since that time a list that includes HEMs is constantly growing, and nowadays high-entropy oxides [10–13], borides [14–17], carbides [18–21], silicides [22–25], sulfides [26–29], nitrides [30–33] etc. have been successfully synthesized. Among HEMs, carbides and carbonitrides containing transition metals of groups IV and V stand out due to their potentially high melting point and chemical stability under extreme conditions, as well as mutual complete solubility between each of them (except VC) [34,35]. In this system, TiZrNbHfTaC<sub>5</sub> stands out as an ideal high-entropy carbide (HEC) with an NaCl-type cubic crystal lattice and the most potential candidate material for structural elements in high-temperature applications due to its high mechanical properties and temperature stability [36,37]. Moreover, there is evidence that the introduction of nitrogen into the structure of HEC can further enhance its performance [38–40], although this is a difficult task.

Most of the available scientific works devoted to the synthesis of TiZrNbHfTaC<sub>5</sub> and the study of its properties represent a two-stage approach consisting of high-energy ball milling of initial precursors followed by ceramics sintering mainly with the SPS method [41–44]. It is worth noting that the reduction of sintering temperatures is achieved by introducing silicon carbide, which forms the matrix under heating conditions [45,46]. Changes in sintering parameters (temperature, heating rate, exposure time) and/or introducing different mass amounts of silicon carbide additives lead to ambiguity of the obtained results and significant variation in the final characteristics: nanohardness – from 35.5 to 38.5 GPa; microhardness – from 16.2 to 32.1 GPa; Young modulus – from 438 to 562 GPa [41–43,45,46]. Such results do not allow estimating the actual values of physical and mechanical characteristics of TiZrNbHfTaC<sub>5</sub>. Moreover, the applicability of ceramic products and the application of energy-consuming multistage processes also raise questions.

An alternative option for obtaining products based on high-entropy materials is the formation of coatings. Despite the increasing number of published works associated with HEC coatings formation during the last few years [47–50], this direction still remains poorly studied, while the HECHN coatings were poorly reported [51–53], especially for Ti-Zr-Nb-Hf-Ta composition [54]. At the same time, the formation of coatings has a significant advantage over the application of ceramics, as it allows modifying the mechanical characteristics of metal substrates without changing their structure and machinability, thus facilitating further application in aggressive conditions. To date, the priority in the formation of HEC and HECHN coatings and thin films is given to magnetron sputtering [55–57], laser cladding [58] and thermal plasma spraying [59,60], since it is necessary to create high-energy impact on

refractory precursors to form the required structure on the substrate surface. One of the varieties of plasma spraying technologies is plasma dynamic synthesis, which, as it was shown in the example of binary and even ternary compounds [61,62], results in producing highly adhesive coatings by spraying pulsed arc discharge plasma. High temperatures ( $> 10,000$  K), sputtering and crystallization rates ( $> 1$  km/s and  $> 10^7$  K/s, respectively), in general, should provide the necessary conditions for depositing and forming HEC and HECHN coatings.

This work is aimed at producing high-entropy carbide TiZrNbHfTaC<sub>5</sub> and carbonitride (TiZrNbHfTa)C<sub>x</sub>N<sub>y</sub> in the form of coatings. The fundamental novelty of this study is that the combination of metal atoms in an equimolar ratio and carbon (as well as nitrogen) into a multi-component compound occurs in a high-speed jet of pulsed arc discharge plasma. The first demonstration of the possibility of stabilizing a high-entropy compound on a metal substrate in the form of a coating made it possible to directly measure the physical and mechanical characteristics and oxidation resistance of the product. The potential elastic and mechanical properties of simulated HEC, HECHN, and HEN single crystals by using different models allowed for control and comparison of the characteristics of the synthesized coatings.

## 2. Materials and methods

### 2.1. Synthesis of high-entropy coatings

Synthesis and deposition of high-entropy (TiZrNbHfTa)C<sub>x</sub>N<sub>y</sub> coatings are carried out by the plasma dynamic method, which consists of using a high-speed arc discharge plasma jet as a medium for high-energy plasma-chemical synthesis reactions. The arc discharge is directly formed with a coaxial magnetoplasma accelerator (Fig. 1a) when a pulsed capacitive energy storage device ( $W_{\max} = 27$  kJ,  $U_{\max} = 3.0$  kV,  $C_{\max} = 6.0 \mu\text{F}$ ) starts feeding the accelerator. This leads to a thermal breakdown of the interelectrode gap (plasma formation zone 4) formed mechanically in the structure of the central electrode insulator 2, which separates the graphite insert of the central electrode 1 and the graphite accelerating channel of the barrel electrode 5. The main reaction precursors are preliminarily placed in this plasma formation zone (Fig. 1b). The thermal effect of the formed arc discharge on the mixture of precursors results in their conversion to a plasma state. Due to the internal magnetic field of arc discharge current and the external magnetic field of the inductor, the plasma jet accelerates and flows into a working chamber filled with an inert gas (argon) or nitrogen at room temperature and atmospheric pressure. To form coatings of high-entropy compounds, a copper plate (grade M1, Cu > 99.9 wt%) is installed on the plasma jet flow path at a distance of 65 mm from the edge of the accelerator. The

**Table 1**  
Ratios of components in prepared precursor mixtures.

Mixture	<i>m</i> , g	Ti	Zr	Nb	Hf	Ta	C
Me	0.121	0.231	0.236	0.453	0.459	—	
Me+C	0.110	0.210	0.214	0.411	0.417	0.138	

choice of copper as a substrate material is due to its high thermal conductivity (387 W/m•K) that contributes to accelerated quenching and crystallization of the coating material.

Pre-preparation of the precursors includes grinding and mixing the components to the required mass ratio. For coating formation, pure metal powders of Ti, Zr, Nb, Hf, and Ta (Rare Metals Corp., Russia, purity 99.9 %, average size  $\leq 10\mu\text{m}$ ) are applied. Sibunit (Federal Research Center Boreskov Institute of Catalysis, Russia, purity 99.0 %,

**Table 2**  
Parameters of the experiments on the synthesis of high-entropy compounds in the form of coatings.

Potential compound	Exp. no.	Mixture	Medium	<i>U</i> <sub>max</sub> , kV	<i>I</i> <sub>max</sub> , kA	<i>P</i> <sub>max</sub> , MW	<i>W</i> , kJ	<i>t</i> <sub>imp</sub> , $\mu\text{s}$	<i>P</i> <sub>av</sub> , MW
HEC	1	Me+C	Ar	1.25	100.80	126.28	20.06	310.00	64.72
HECN	2	Me+C	N <sub>2</sub>	1.30	99.00	128.62	20.01	320.00	62.53
HEN	3	Me	N <sub>2</sub>	1.37	99.00	135.51	19.10	310.00	61.61

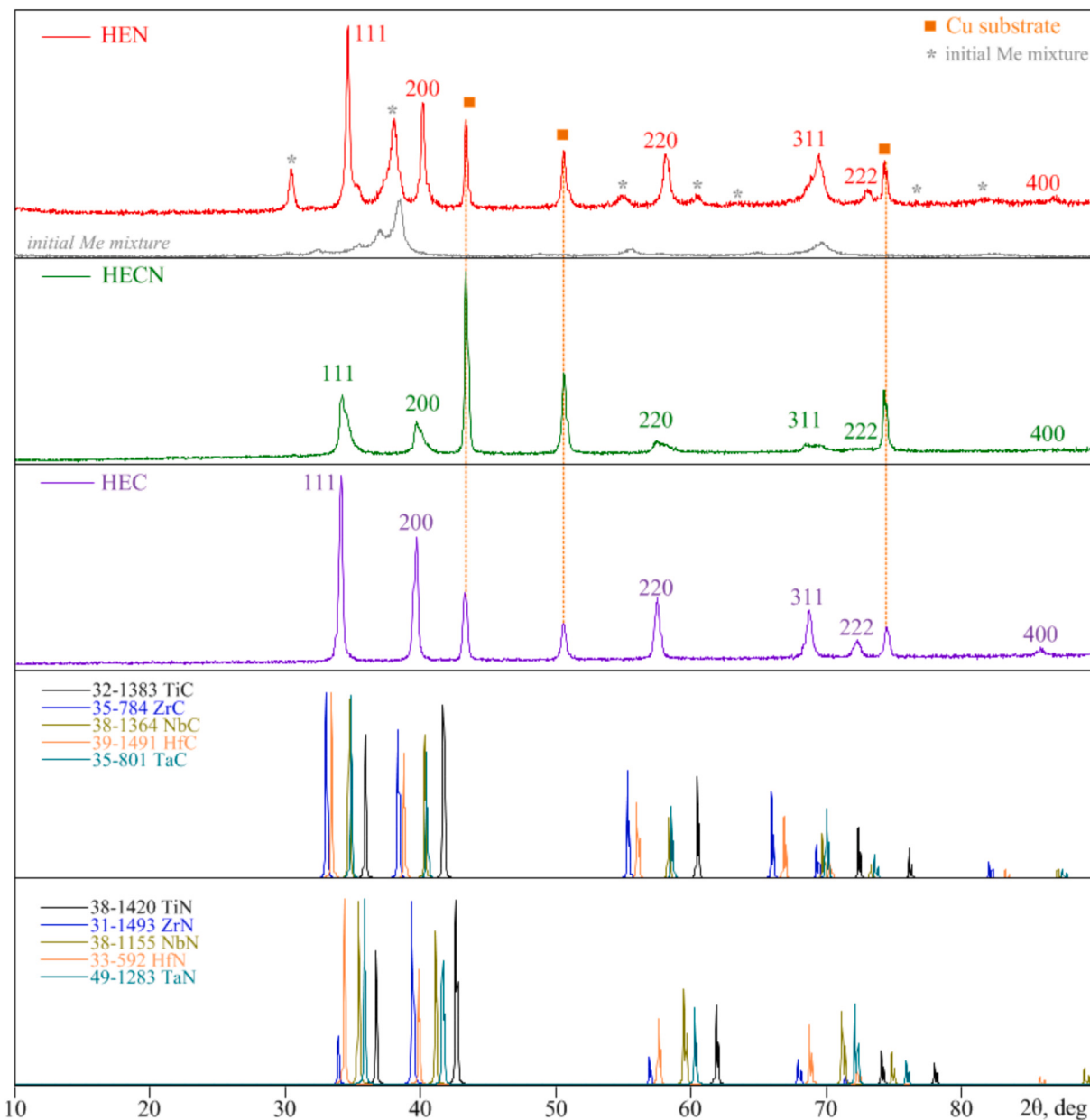


**Fig. 2.** X-ray diffraction patterns of HEC, HECH, and HEN coatings obtained in the graphite electrode system from the raw powder of individual metals in comparison with reference XRD patterns of individual carbides and nitrides.

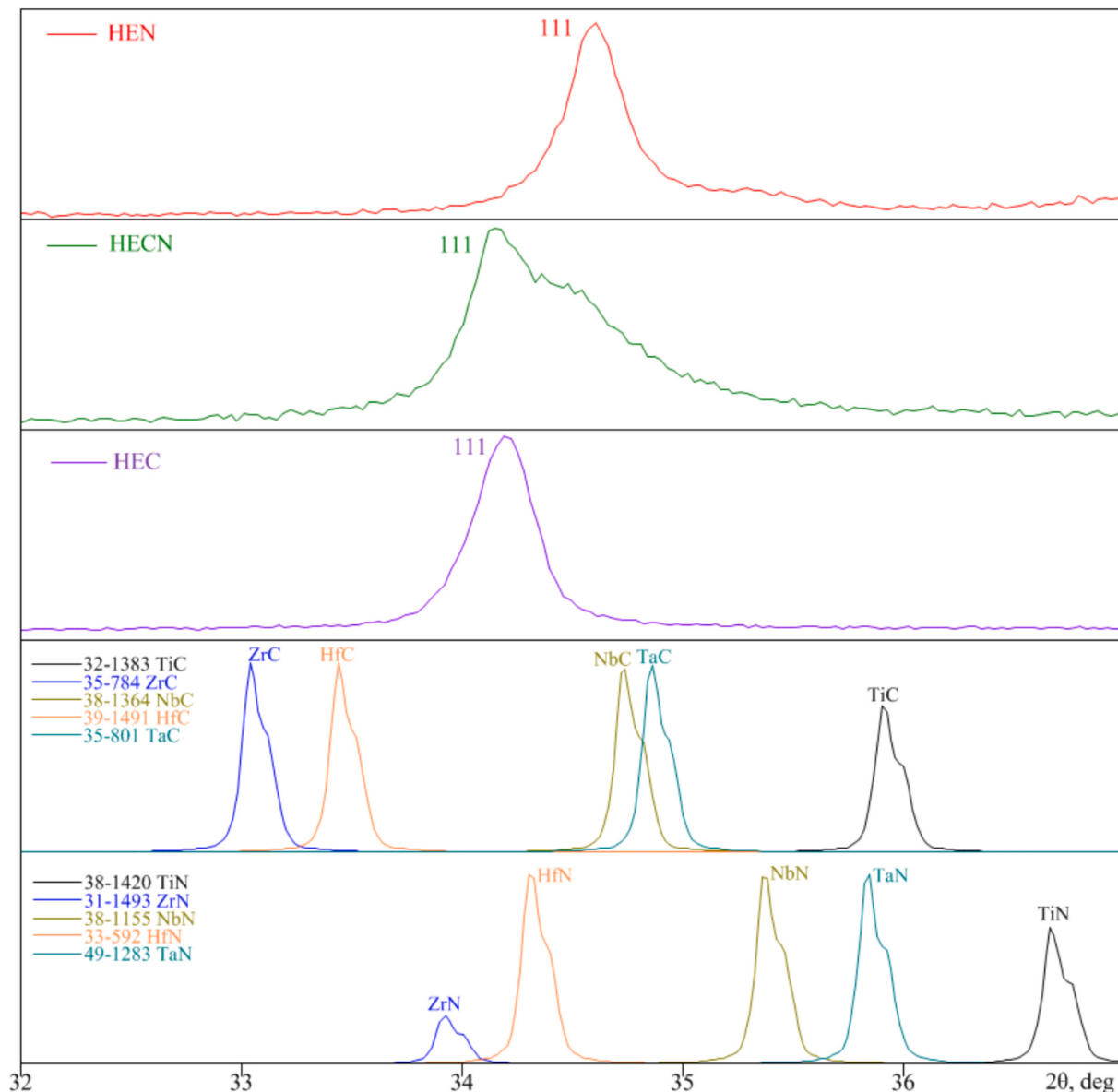


**Fig. 3.** X-ray diffraction patterns of HEC, HEON, and HEN coatings obtained in a graphite electrode system the raw powder of individual metals in comparison with reference XRD patterns of individual carbides and nitrides (diffraction angle  $2\theta = 32\text{--}37$  deg. near peak 111).

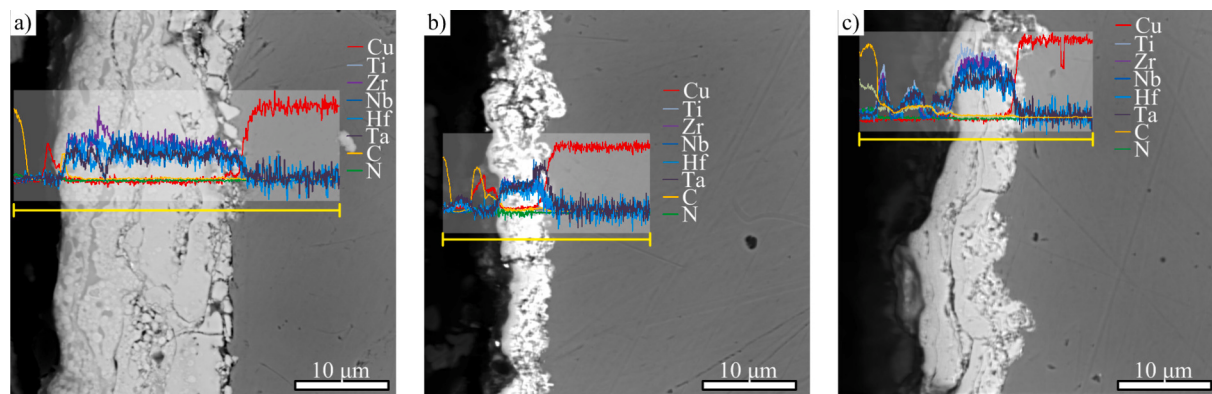


**Fig. 4.** SEM images with the corresponding EDS data for coatings synthesized in HEC (a), HEON (b), and HEN (c) series.

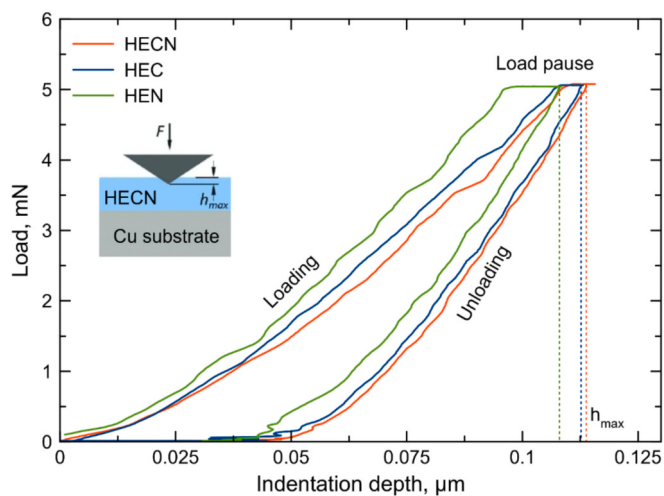


**Fig. 5.** Indentation curves of studied HEC (blue), HECHN (orange), and HEN (green) coatings on Cu substrates. Maximum load is 5 mN. (For interpretation of the references to colour in this figure legend, the reader is referred to the web version of this article.)

**Table 3**

Measured hardness and Young's modulus of obtained coatings in comparison with calculated ones for HEC, HECHN, and HEN. Hardness values were calculated using Chen's [85] ( $H_V^C$ ), and Mazhnik-Oganov [86] ( $H_V^{MO}$ ) models, respectively.

Name	Nitrogen concentration C/(C + N)	$H_V$ (exp), GPa	$H_V^C$ (DFT), GPa	$H_V^{MO}$ (DFT), GPa	E (exp), GPa	E (DFT), GPa
HEC	0	31.9	26.69	23.20	303.2	457.72
	0.125		26.04	22.60		454.59
	0.25		26.26	22.72		451.25
	0.375		24.06	20.87		437.61
	0.5		21.76	19.39		419.17
	0.625		21.05	19.05		413.63
	0.75		19.03	18.29		396.47
HECN	0.875	31.5	16.90	18.02	320.5	382.28
HEN	1	34.7	14.01	17.44	304.2	354.29

surface area  $\sim 340 \text{ m}^2/\text{g}$ ) plays the role of a carbon source. Table 1 represents the ratios of components in specific powder mixtures to achieve equiatomic metal content, as well as a five-fold atomic carbon content for the possible formation of the  $(\text{TiZrNbHfTa})_{0.5}\text{N}_{0.5}$  structure. The equiatomic selection of metals corresponds to the traditional concept of

high-entropy materials [63]. The initial powders were mixed and activated mechanically for 10 h using a Mixer/Mill 8000 M ball mill (SPEX Sample Prep, USA) in a  $\text{ZrO}_2$  grinding vessel and with two balls made of the same material. The supporting information file (Fig. S1-S2) contains micrographs and X-ray diffraction patterns of the initial components and their mixtures, demonstrating the reactionless formation of the  $\text{Ti-Zr-Nb-Hf-Ta-(C)}$  mixture at the mechanical processing stage. The initial metals differ in granulometric composition (Fig. S3, supporting information), but mechanical processing allows grinding large particles, averaging sufficiently the precursor dispersion, and reducing significantly the spread of particle sizes (Fig. S4). In addition to this, during the plasma dynamic method implementation, plasma processing of precursors under extreme energy conditions results in the sublimation of components that differ significantly in size and structure.

For experiments on the synthesis of high-entropy coatings, a graphite-type electrode system is used, since it is distinguished by the possibility of achieving higher temperatures and pressures in the generated plasma (up to 25,000 K and 8 MPa, respectively, at a current of up to 100 kA) [64]. Such parameters of pressures and temperatures make it possible to implement the synthesis of refractory compounds through a liquid-phase state [62,65,66]. It is known precisely that the impossibility of achieving the necessary synthesis conditions is the reason for the unsatisfactory results of the methods used today for the synthesis of high-entropy carbides and their derivatives [67]. In addition, in the pulsed thermal plasma under consideration, efficient homogenization and uniform distribution of atoms are achieved. This leads to the preservation of the equimolar ratio of metals not only in the initial powder mixture but also in the resulting coating.

Discharge current and voltage during synthesis are recorded using Tektronix TDS2012 oscilloscopes through the Rogowski coil and ohmic voltage divider, respectively. The recorded data are used to calculate energy characteristics such as maximum arc voltage ( $U_{\max}$ ), amplitude of discharge current ( $I_{\max}$ ), amplitude of discharge power ( $P_{\max}$ ), value of energy released ( $W$ ), pulse duration ( $t_{\text{imp}}$ ), and average value of discharge power ( $P_{\text{av}}$ ). The main energy parameters recorded when conducting a series of experiments on high-entropy coatings deposition are represented in Table 2.

## 2.2. Materials characterization

The phase composition of initial raw materials is analyzed by X-ray diffraction methods using a Shimadzu XRD-7000 X-ray diffractometer 7000 ( $\text{CuK}\alpha 1$ -irradiation,  $\lambda_1 = 1.5406 \text{ \AA}$ ,  $2\theta = 10\text{--}90 \text{ deg}$ ). Diffraction reflections are identified using the Crystallographica Search-Match program and the PDF4+ structure database. The average value of the lattice constant  $a$  of high-entropy compounds with a cubic structure is

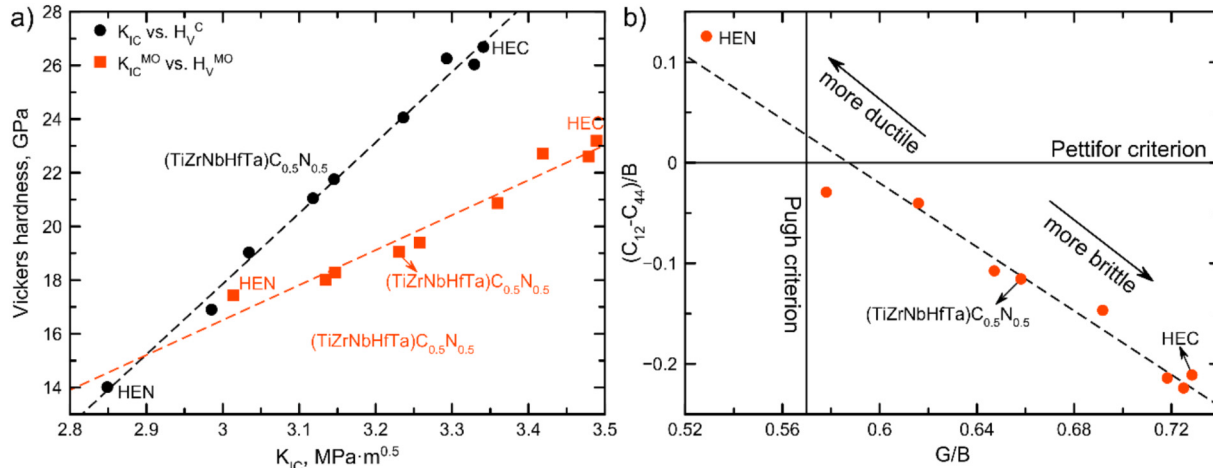


**Fig. 6.** Ashby plot in the coordination of Vickers hardness and fracture toughness ( $K_{IC}$ ) (a) and Pugh-Pettifor criterion for considered HECN structures (b).

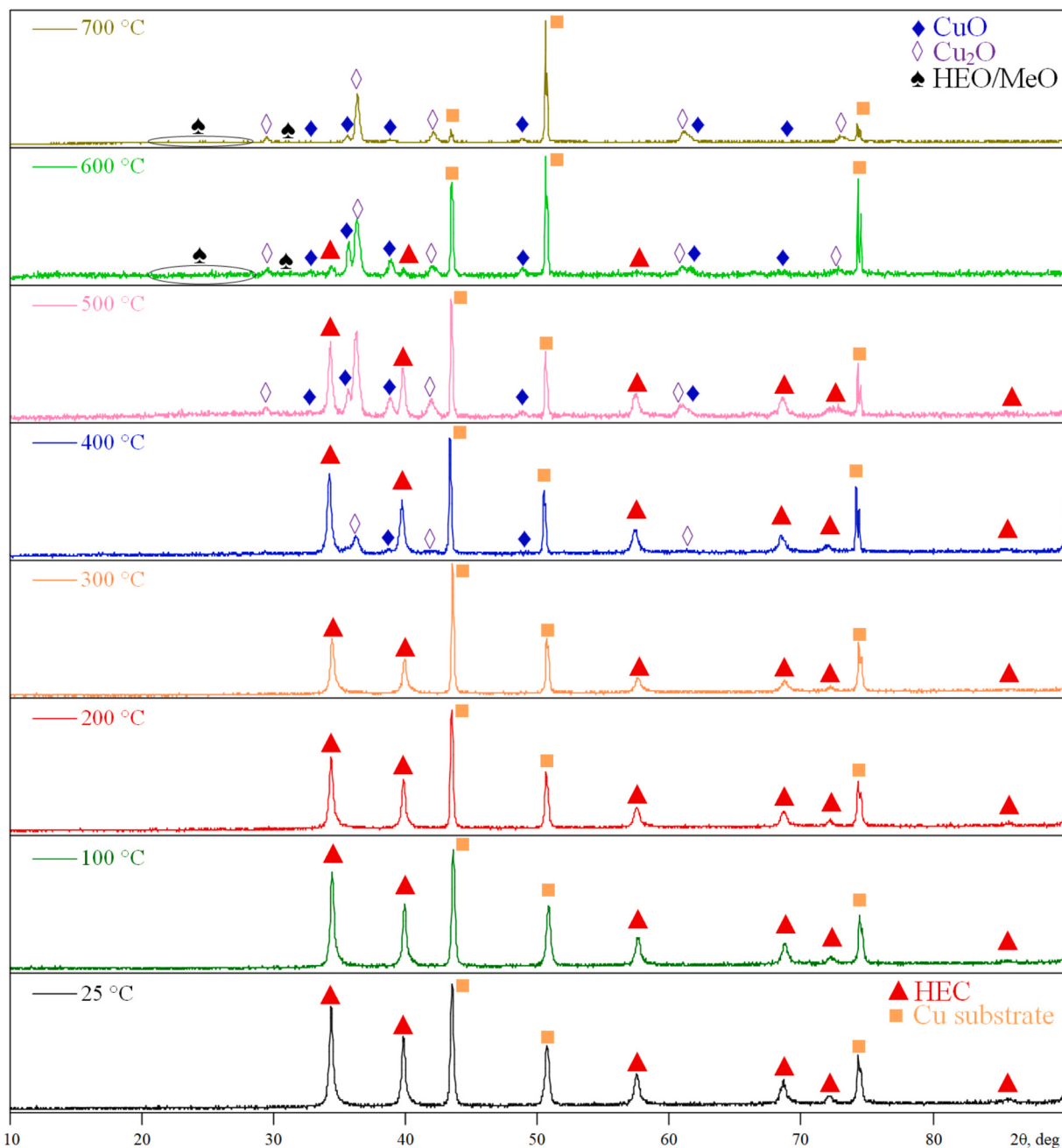


**Fig. 7.** XRD-patterns of coatings obtained in a graphite electrode system from a mixture of Me (HEC series) under the conditions of temperature increase.

determined from the position of the X-ray maxima  $2\theta_{hkl}$  with Miller indices (111), (200), (220), (311), (222), (400) and the corresponding interplanar distances  $d_{hkl}$ . When studying the coatings using the XRD method, an asymmetrical geometry in the sliding beam mode is used to avoid the substrate influence on the determination of the X-ray maximum position (fixed incident beam tilt angle  $\theta_1 = 3^\circ$  and reflected beam angle  $\theta_2 = 10\text{--}90^\circ$ ).

The microstructure and properties of high-entropy coatings are studied after additional processing. To obtain the transverse coating profile, a polished section is prepared. For this purpose, a  $5 \times 5$  mm sample is cut out from a coated sample and then placed in a casting mold. This sample is poured with a special Technovit 5000 casting compound in a position perpendicular to the horizontal surface. After hardening, the sample is processed using a Forcipol 1 V grinding and polishing machine by using SiC 320, 600, 800, and 1200 grinding papers and then by 6, 3, 1, and 0.25  $\mu\text{m}$  polishing cloths and appropriate

diamond suspensions and lubricants.

To study the microstructure of the coating sections, the scanning electron microscopy analysis is performed using a Hitachi TM3000 microscope and both Tescan Mira 3LMU and Quanta 200 3D with X-ray energy-dispersive microanalysis systems.

The physical and mechanical properties are studied by nanoindentation using a Table Top Nanoindentation Tester (TTX-NHT) with a Vickers pyramid at a load of 5 mN and a loading rate of 10 mN/min. Indenter prints are applied in accordance with the method described in ASTM C1327-15 (2019). As a result, the values of nanohardness and Young's modulus are calculated from the loading-unloading curves (Oliver-Pharr method).

The oxidation properties are studied using direct annealing in a P310 Nabertherm atmospheric furnace with a heating rate of 10  $^\circ\text{C}/\text{min}$ . The holding time at the required maximum temperature is 10 min. Annealing of each coating is performed sequentially to temperatures of 100,

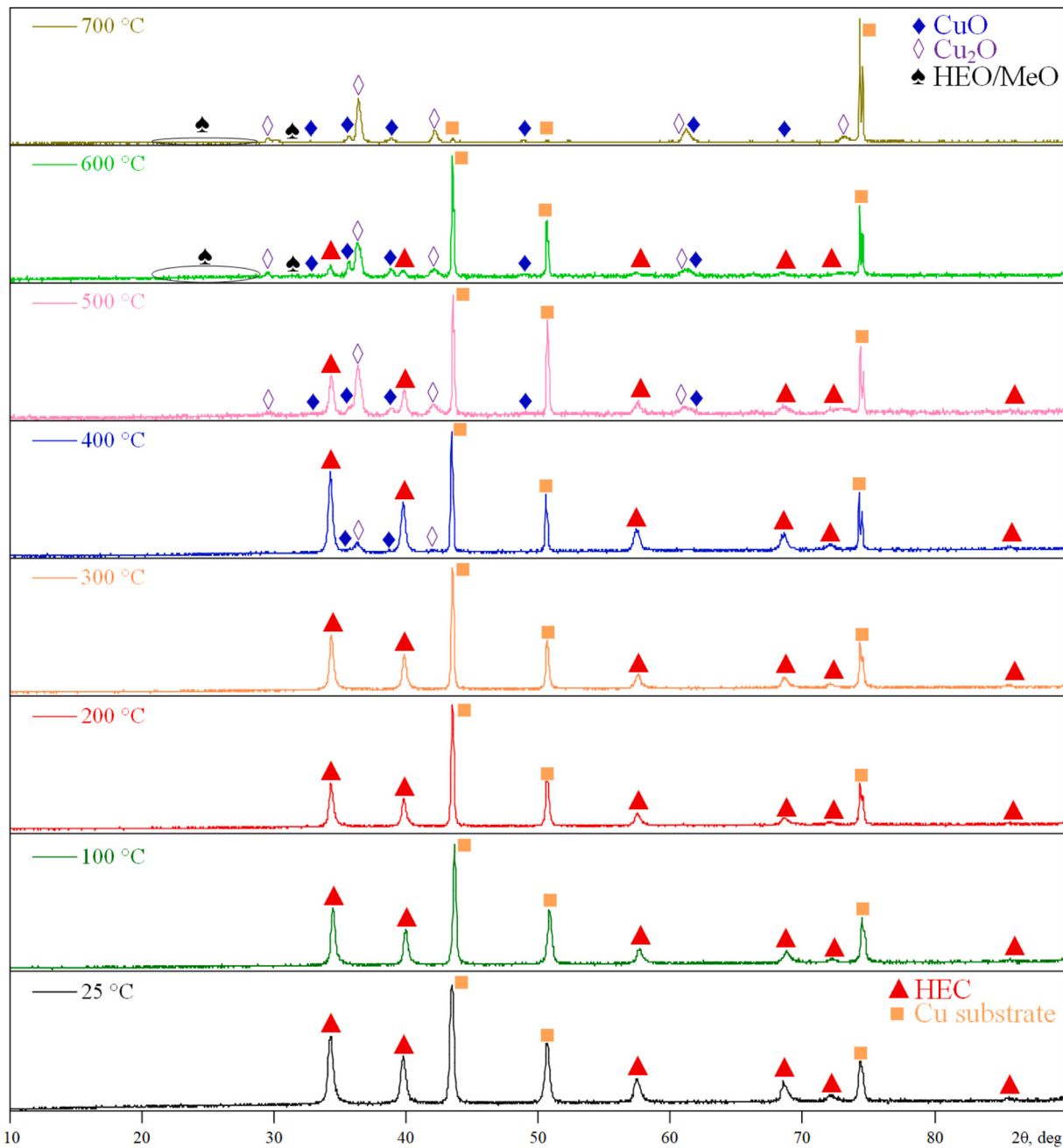


**Fig. 8.** XRD-patterns of coatings obtained in a graphite electrode system from a mixture of Me (HECN series) under the conditions of temperature increase.

200, 300, 400, 500, 600, 700 °C, after which the X-ray diffraction patterns are recorded.

### 2.3. Computational details

Our calculations are based on the density functional theory (DFT) [68,69] within the generalized gradient approximation (the Perdew–Burke–Ernzerhof functional) [70] and the projector augmented wave method [71,72] as implemented in the VASP [73–75] code. The plane wave energy cutoff of 400 eV, the Methfessel–Paxton smearing [76] of electronic occupations, and  $\Gamma$ -centered  $k$ -point meshes with a resolution of  $2\pi \times 0.025\text{\AA}^{-1}$  for the Brillouin zone sampling were used, ensuring the convergence of the energy differences and stress tensors.

### 3. Results and discussion

To demonstrate the potential of plasma dynamic method for the synthesis of high-entropy compounds in the form of coatings, a series of experiments was performed to obtain carbide and presumably carbonitride based on Ti–Zr–Nb–Hf–Ta. A mixture of metals Ti, Zr, Nb, Hf, Ta was applied as synthesis precursors, while experiments were performed in argon (HEC) and in nitrogen with additional carbon (HECN) and without carbon (HEN). For the resulting coatings, the X-ray diffraction patterns were measured as shown in Fig. 2. All the XRD patterns contain the main maxima 111 ( $2\theta \approx 34$  deg), 200 ( $2\theta \approx 40$  deg), 220 ( $2\theta \approx 58$  deg), 311 ( $2\theta \approx 69$  deg), 311 ( $2\theta \approx 73$  deg), 400 ( $2\theta \approx 85$  deg) attributed to a crystalline phase with a face-centred cubic structure and  $Fm\bar{3}m$  (no. 225) space group that proves the formation of high-entropy compound. In all cases, individual metal carbides and nitrides do not form.

The coatings obtained from HEC and HECN are single-phase in

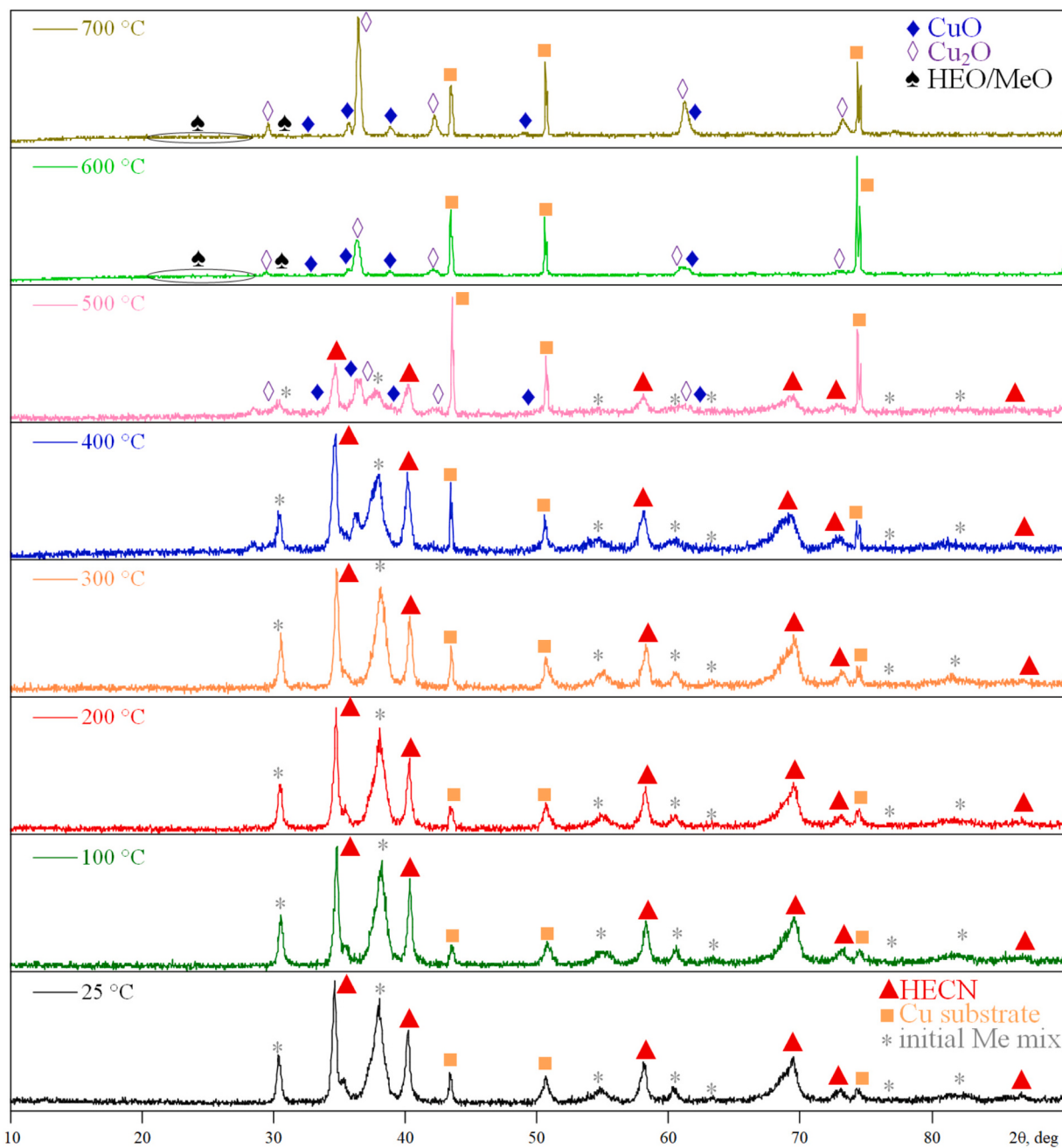


**Fig. 9.** XRD-patterns of coatings obtained in a graphite electrode system from a mixture of Me (HEN series) under the conditions of temperature increase.

nature, if do not take into account the presence of copper peaks from the metal substrate. The XRD-pattern of HEN differs with the presence of additional phases, the maxima of which ( $2\theta \approx 30.4, 38.1, 54.9, 60.5, 63.4, 76.7, 81.7$  deg) correlate well with the XRD-pattern of initial Me mixture. Apparently, the reason for this phenomenon is a significant lack of carbon in the HEN system. In the cases of HEC and HECH, a mixture of metals and Sibunite (as a carbon source) was placed in the plasma formation zone. However, in the case of HEN, no additional carbon was added. So, carbon was only introduced into the system through electrical erosion of the graphite electrodes. For this reason, some initial metals did not react either with nitrogen (due to the strong bonding energy of N<sub>2</sub> molecules, which are difficult to destroy and activate under the considered synthesis conditions) or with carbon (due to its deficiency in the considered experiments).

If analyzing the enlarged region near the intense peak 111 (Fig. 3), the phase identification of synthesized coatings can be done more

accurately. In both HEC and HECH cases, no significant shift of the main intensity maximum toward metal nitrides can be detected. This indicates the predominant formation of high-entropy carbide TiZrNbHfTaC<sub>5</sub>. Table S1 (supporting information) presents the results of calculating the lattice constants of the synthesized cubic crystalline phase, close to the theoretical values according to Vegard's rule and the DFT predicted values. Which also indicates the formation of high-entropy carbide.

As in the case of the HEC and HECH experiments, the HEN experiment (applying the mixture without carbon, medium atmosphere – nitrogen) also produces a cubic structure of the  $Fm\bar{3}m$  type. However, in general, the results of the HEN experiment differ significantly from those of HEC and HECH. First, the formed cubic crystalline phase has a larger shift of the  $a$  parameter toward the calculated value for the high-entropy nitride. The  $a$  values for HEC and HECH are 4.54 Å, for HEN – 4.49 Å, while the theoretical value for the high-entropy nitride (according to Vegard's rule) should be 4.41 Å. Such results may indicate partial

incorporation of nitrogen into the structure and the possible formation of high-entropy carbonitride.

Secondly, when analyzing the X-ray diffraction patterns of the HEN experiment, the presence of peaks (\*) is obvious, which are additional to the main cubic crystalline phase and the copper substrate. These X-ray maxima can be identified with the remains of the initial metal mixture placed in the plasma formation zone. However, compared to XRD-pattern of the initial mixture, some differences are noticeable that indicates the effect exerted on the initial mixture during the plasma jet outflow. Such results can be associated with special conditions arising during the plasma jet interaction with the metal substrate, which were previously discussed in other studies on plasma dynamic synthesis [66]. When the plasma jet flows out of the accelerating channel almost immediately (since the distance from the electrode-barrel cut to the substrate is extremely small) onto the substrate with a priori weak interaction with nitrogen and a low concentration of carbon, some of the precursors do not have time to react with carbon, settling on the substrate in their original form. Under such conditions, high-entropy TiZrNbHfTa alloys can be formed, as well as intermediate phases (bcc Ta—Nb and hcp Hf—Zr), X-ray maxima of which are close enough to those identified in the HEN XRD-pattern [77,78].

The microstructure of the obtained coatings was studied using scanning electron microscopy. Fig. 4 demonstrates BSE mode micrographs of sections of the coatings obtained under different conditions. Contrasting light areas correspond to the chemical elements Ti, Zr, Nb, Hf, and Ta with a high atomic number, presenting in the coating material. The coating thickness varies from 5 to 20  $\mu\text{m}$ , reaching maximum values in the HEC experiment. The synthesized material structure is sufficiently dense and homogeneous with a minimum number of pores and cracks, which is an excellent result for the plasma method of coating formation with a high deposition rate, intense heating and cooling, and the significant difference in the coefficients of linear thermal expansion between the coating and the substrate [79,80]. Fig. 4 also shows the results of EDS analysis along the coating-substrate line in the form of a distribution of the main chemical elements. The EDS results confirm the formation of a coating containing Ti, Zr, Nb, Hf, and Ta.

The totality of the obtained data and the characteristics of the formed coatings are scientifically valuable since there are not too much reliable information on the synthesis of high-entropy nitrides and carbonitrides in a bulk form in the literature [81]. At present, there are only few reports on the production of (TiZrNbHfTa) $X$  ( $X = \text{N}, \text{CN}$ ) compounds in a bulk form [82,83], and studies of such materials are mainly related to modeling their structure, calculating its possible parameters, and predicting probable properties [72]. The production of such crystalline phases in the composition of coatings is very intriguing and allow measuring directly their physical and mechanical properties, as well was oxidation resistance of and the study of their properties.

To demonstrate the mechanical properties of the obtained materials, nanoindentation of the coating layers was performed. Fig. 5 presents the indentation curves for three samples, namely HEC, HECN, and HEN. Indentation load was 5 mN. One can clearly see the loading and unloading regions, where the maximal achieved indentation depths were 0.112, 0.113, and 0.108  $\mu\text{m}$  for HEC, HECN, and HEN, respectively. The obtained values of Vickers hardness of the HEC and HECN series coatings are shown in Table 3 and correspond to the known values for materials of the composition HfNbTaTiZrC<sub>5</sub> with  $H_V \approx 32$  GPa, while reported theoretical values have even lower values  $H_V = 27\text{--}29$  GPa [84].

Estimated hardness of simulated single crystals of HEC, HECN, and HEN by using Chen's [85] ( $H_V^C$ ), and Mazhnik-Oganov [86] ( $H_V^{MO}$ ) models, are also added to the Table 3 for comparison. The more detailed information about potential mechanical properties is given in table S2 (supporting information). Calculated Vickers hardness according to Chen's model for HEC is about 26 GPa, while Mazhnik-Oganov model gives 23 GPa. Both models are in good agreement with experimentally

measured values. The hardness values of the synthesized coatings exceed the hardness of individual carbides  $H_V(\text{TiC}) = 31\text{--}32$  GPa,  $H_V(\text{ZrC}) = 23\text{--}25$  GPa,  $H_V(\text{NbC}) = 19\text{--}25$  GPa,  $H_V(\text{HfC}) = 19\text{--}25$  GPa,  $H_V(\text{TaC}) = 16\text{--}23$  GPa. The obtained values of Young's modulus of coatings ( $E$ ) is in the range of 303–321 GPa were lower than the theoretical calculated values ( $E = 457$  GPa), but significantly higher than the known experimental values of  $E = 188$  GPa [84].

The difference in physical and mechanical properties demonstrated by the HEN sample is the increase in hardness to 34.7 GPa. The most obvious reason for the increase in hardness is the introduction of nitrogen atoms into the structure of the material and the probable formation of carbonitride (or local nitride). It is known that many transition metal carbonitrides have a slight decrease in hardness when replacing carbon atoms with nitrogen [87]. However, ternary nitrides and carbonitrides with more principal elements turn out to be superstrong, i.e. harder, and more ductile than binary systems, due to the optimal concentration of valence electrons in the range  $\text{VEC} = 9.0\text{--}10.0$  [88]. As a result, for such high-entropy nitrides and carbonitrides, the hardness can increase by 20 % and 40 %, respectively, compared to monocarbides and mononitrides [89]. For such systems, the confirmed experimental hardness is up to 31 GPa for ternary nitrides [90,91] and up to 33 GPa for the high-entropy compound  $(\text{Hf}_{0.2}\text{Nb}_{0.2}\text{Ta}_{0.2}\text{Ti}_{0.2}\text{Zr}_{0.2})\text{N}$  [92]. Thus, the coatings synthesized and investigated in our work showed even higher hardness values than previously reported in the literature.

Theoretically predicted hardness for HEN by both empirical models indicate lower values compared to experimental data. Hardness for  $(\text{TiZrNbHfTa})\text{N}$  was predicted to be even lower than for  $(\text{TiZrNbHfTa})\text{C}_{0.125}\text{N}_{0.875}$  (Table 2). The reason of such discrepancy in the obtained data for nitrides and complex compounds with nitrogen is known for empirical models and is related to the incorrect description of strong N—N bonds compared to other less strong bonds in the structure [93].

Further analysis of mechanical properties by DFT methods is made via construction of Ashby plots for Vickers hardness and fracture toughness (Fig. 6a). Hardness and fracture toughness are calculated using empirical models. Such relations allow us to analyze the influence of nitrogen concentration on the ductility and brittleness of considered HECN. One can see that predicted Vickers hardness of HECNs decreases as the nitrogen content increases, Fig. 6a. Fracture toughness decreases from 3.5 to 3  $\text{MPa}\cdot\text{m}^{0.5}$ . Similar situation observed for fracture toughness, i.e. increased nitrogen content decreases the fracture toughness. So general trend for mechanical properties is degradation of both hardness and fracture toughness during change of nitrogen content from HEC to HEN.

Pugh-Pettifor criterion is shown in Fig. 6b. Here one can see that increase in the nitrogen content leads to more ductile behavior for HECN. Brittleness of high-entropy carbonitride increases as the carbon content increases, see Fig. 6b. Addition of nitrogen can be considered as a way for tuning the mechanical properties of high-entropy carbide making them less brittle and more ductile, which is important for some special applications in mining.

In addition to modeling, predicting and measuring the physical and mechanical properties, the oxidation resistance of the synthesized coatings at elevated temperatures are studied. Fig. 7–9 represent XRD-patterns of the coatings heated to temperatures from 100 to 700 °C in comparison with the initial product of plasma dynamic synthesis (25 °C). Based on the presented data, it is possible to identify phase transformations occurring with coatings of high-entropy materials at elevated temperatures. It is worth noting that, in general, the oxidation properties of all synthesized coatings are similar. Thus, regardless of the composition, approximately the same onset of oxidation processes is observed for both the metal substrates and the HEC/HECN compounds themselves. Up to 300 °C, no phase changes are observed in the materials. The XRD patterns after 400 °C show the formation of copper oxides in the form of the predominant cuprite  $\text{Cu}_2\text{O}$  (ICDD 00–005–0667) and additionally tenorite  $\text{CuO}$  (ICDD 00–045–0937) phases. Despite substrate oxidation, the main cubic structure in the coating remains

unchanged. With further heating, an increase in the intensity of the peaks of the Cu—O crystalline phases is observed.

Phase changes in the coating are observed at a temperature of 600 °C. At this point, a sharp decrease in the intensity of the peaks of carbide/carbonitride compounds begins. At the same time, the appearance of low-intensity and strongly broadened maxima can be observed that can indicate the formation of hypothetical high-entropy oxides [94]. Another oxidation way of high-entropy HEC/HECN is the formation of more stable crystalline phases with a monoclinic and orthorhombic structure  $\text{AB}_2\text{O}_7$  and  $\text{A}_6\text{B}_2\text{O}_{17}$ , respectively, where A = Ti, Zr, and Hf, B = Nb, Ta [95]. The low intensity and broadening of the oxide peaks can be associated with their X-ray amorphous structure. At a temperature of 700 °C, peaks associated with the initial cubic structure of the coating are absent that indicates the completion of the oxidation process.

The revealed results indicate a sufficiently high oxidation resistance of the formed HEC/HECN coatings, allowing one to consider them not only as strengthening ones, but also as protective for application in various aggressive environments. It should be taken into account that the data on thermal studies of bulk HEC/HECN materials are extremely limited and often highly contradictory. The presented results make a significant contribution to understanding the behavior of such materials in the temperature course and make it possible to assess their potential in high-temperature applications. In general, the developed approach with the prediction of the material properties of materials, their synthesis by the plasma dynamic method and verification of a set of physical and mechanical properties can allow expanding the understanding of high-entropy materials, including hypothetical compounds. The current coating on a copper substrate can be used to improve the mechanical properties and thermal stability of the metal surface by applying a harder and more refractory compound.

#### 4. Conclusion

In the present study, we develop a technique based on the application of plasma dynamic method to obtain high-entropy materials in the form of a coating. The main findings are summarized as follows:

- (1) The developed technique based on the application of a high-speed arc discharge plasma jet provides the formation of high-entropy carbides  $\text{TiZrNbHfTaC}_5$  and carbonitrides  $(\text{TiZrNbHfTa})\text{C}_x\text{N}_y$  coatings with the thickness up to 20 μm.
- (2) The key feature of the obtained IV-V transition metal compounds is shown to be the synthesis of a cubic crystalline phase ( $Fm\bar{3}m$  space group, fcc structure) without any impurities, regardless of the synthesis conditions.
- (3) When using a carbon-free mixture of precursors and nitrogen as a gas medium, it is possible to obtain the HECN coatings on the copper plate that is capable of demonstrating hardness values up to ~35 GPa, which exceeds those for HEC (~32 GPa).
- (4) The resulting HEC/HECN coatings demonstrate sufficiently high oxidation resistance (up to 700 °C), which in combination with high hardness indicates the possibility of using the obtained materials not only to create heat-resistant products, but also strengthen them significantly.

The implications and importance of this work extend far beyond the results shown herein since it is possible to construct many hundred combinations of group 4, 5 and 6 transition metals in high-entropy carbides or carbonitrides. By forming corresponding coatings based on high-entropy materials it is possible to discover the potential properties for a wide range of high-entropy compositions.

#### CRediT authorship contribution statement

**Dmitry S. Nikitin:** Conceptualization, Data curation, Methodology, Writing – original draft. **Ivan I. Shanenkov:** Conceptualization, Methodology, Writing – original draft. **Artur Nassyrbayev:** Data curation, Formal analysis, Investigation. **Alexander A. Sivkov:** Supervision, Writing – review & editing. **Viktor S. Baidyshev:** Formal analysis, Investigation, Validation. **Yulia A. Kvashnina:** Data curation, Formal analysis, Visualization. **Nikita A. Matsokin:** Data curation, Formal analysis, Investigation. **Alexander Ya. Pak:** Conceptualization, Funding acquisition, Supervision. **Alexander G. Kvashnin:** Conceptualization, Methodology, Supervision, Writing – original draft.

#### Declaration of competing interest

The authors declare that they have no known competing financial interests or personal relationships that could have appeared to influence the work reported in this paper.

#### Acknowledgments

The study was supported by the Ministry of Science and Higher Education of the Russian Federation (project No. FSWW-2025-0003).

#### Appendix A. Supplementary data

Supplementary data to this article can be found online at <https://doi.org/10.1016/j.ijrmhm.2025.107537>.

#### Data availability

Data will be made available on request.

#### References

- [1] P. Sarker, T. Harrington, C. Toher, C. Oses, M. Samiee, J.-P. Maria, D.W. Brenner, K.S. Vecchio, S. Curtarolo, High-entropy high-hardness metal carbides discovered by entropy descriptors, *Nat. Commun.* 9 (2018) 4980, <https://doi.org/10.1038/s41467-018-07160-7>.
- [2] W. Zhang, D. Yan, W. Lu, Z. Li, Carbon and nitrogen co-doping enhances phase stability and mechanical properties of a metastable high-entropy alloy, *J. Alloys Compd.* 831 (2020) 154799, <https://doi.org/10.1016/j.jallcom.2020.154799>.
- [3] P. Zhang, X. Liu, A. Cai, Q. Du, X. Yuan, H. Wang, Y. Wu, S. Jiang, Z. Lu, High-entropy carbide-nitrides with enhanced toughness and sinterability, *Sci. China Mater.* 64 (2021) 2037–2044, <https://doi.org/10.1007/s40843-020-1610-9>.
- [4] Q. Fu, L. Zhuang, Q. Ren, L. Feng, H. Li, Y. Guo, Carbon nanotube-toughened interlocking buffer layer to improve the adhesion strength and thermal shock resistance of SiC coating for C/C-ZrC-SiC composites, *J. Mater.* 1 (2015) 245–252, <https://doi.org/10.1016/j.jmat.2015.07.006>.
- [5] S. Chen, J. Wang, Z. Chen, W. Song, Y. Zeng, X. Li, T. Li, X. Xiong, Nb- and Ta-doped  $(\text{Hf}, \text{Zr}, \text{Ti})\text{C}$  multicomponent carbides with enhanced oxidation resistance at 2500 °C, *J. Adv. Ceram.* 13 (2024) 332–344, <https://doi.org/10.26599/JAC.2024.9220856>.
- [6] J. Wei, X. Chu, X. Sun, K. Xu, H. Deng, J. Chen, Z. Wei, M. Lei, Machine learning in materials science, *InfoMat* 1 (2019) 338–358, <https://doi.org/10.1002/inf2.12028>.
- [7] T. Mueller, A.G. Kusne, R. Ramprasad, Machine Learning in Materials Science, 2016, pp. 186–273, <https://doi.org/10.1002/9781119148739.ch4>.
- [8] J.-W. Yeh, S.-K. Chen, S.-J. Lin, J.-Y. Gan, T.-S. Chin, T.-T. Shun, C.-H. Tsau, S.-Y. Chang, Nanostructured high-entropy alloys with multiple principal elements: novel alloy design concepts and outcomes, *Adv. Eng. Mater.* 6 (2004) 299–303, <https://doi.org/10.1002/adem.200300567>.
- [9] B. Cantor, I.T.H. Chang, P. Knight, A.J.B. Vincent, Microstructural development in equiatomic multicomponent alloys, *Mater. Sci. Eng. A* 375–377 (2004) 213–218, <https://doi.org/10.1016/j.msea.2003.10.257>.
- [10] A.H. Phakatkar, M.T. Saray, M.G. Rasul, L.V. Sorokina, T.G. Ritter, T. Shokuhfar, R. Shahbazian-Yassar, Ultrafast synthesis of high entropy oxide nanoparticles by flame spray pyrolysis, *Langmuir* 37 (2021) 9059–9068, <https://doi.org/10.1021/acs.langmuir.1c01105>.
- [11] T.D. Desissa, M. Meja, D. Andoshe, F. Olu, F. Gochole, G. Bekele, O.A. Zelekew, T. Temesgen, B. Brehane, K.D. Kuffi, T. Hunde, Synthesis and characterizations of  $(\text{Mg}, \text{Co}, \text{Ni}, \text{Cu}, \text{Zn})\text{O}$  high-entropy oxides, *SN Appl. Sci.* 3 (2021) 733, <https://doi.org/10.1007/s42452-021-04724-z>.

- [12] M. Anandkumar, E. Trofimov, Synthesis, properties, and applications of high-entropy oxide ceramics: current progress and future perspectives, *J. Alloys Compd.* 960 (2023) 170690, <https://doi.org/10.1016/j.jallcom.2023.170690>.

[13] J. Zhang, J. You, Y. Zhao, T. Liu, High-entropy oxides as promising electrocatalysts for oxygen evolution reaction: a review, *J. Environ. Chem. Eng.* 13 (2025) 116550, <https://doi.org/10.1016/j.jece.2025.116550>.

[14] B. Storr, D. Kodali, K. Chakrabarty, P.A. Baker, V. Rangari, S.A. Catledge, Single-step synthesis process for high-entropy transition metal boride powders using microwave plasma, *Ceramics* 4 (2021) 257–264, <https://doi.org/10.3390/ceramics4020020>.

[15] X. Zhang, W. Li, H. Tian, J. Liu, C. Li, H. Dong, J. Chen, M. Song, B. Chen, H. Sheng, S. Wang, D. Zhang, H. Zhang, Ultra-incompressible high-entropy diborides, *J. Phys. Chem. Lett.* 12 (2021) 3106–3113, <https://doi.org/10.1021/acs.jpclett.1c00399>.

[16] B. Storr, L. Moore, K. Chakrabarty, Z. Mohammed, V. Rangari, C.-C. Chen, S. A. Catledge, Properties of high entropy borides synthesized via microwave-induced plasma, *API Mater.* 10 (2022), <https://doi.org/10.1063/5.0098276>.

[17] S. Iwan, C. Perreault, Y.K. Vohra, Synthesis and ultrahigh pressure compression of high-entropy boride ( $Hf_0.2Mo_0.2Nb_0.2Ta_0.2Zr_0.2B_2$ ) to 220 GPa, *Materials* 16 (2022) 158, <https://doi.org/10.3390/ma16010158>.

[18] A.Ya. Pak, V. Sotskov, A.A. Gumovskaya, Y.Z. Vassilyeva, Z.S. Bolatova, Y. A. Kvashnina, G.Ya. Mamontov, A.V. Shapeev, A.G. Kvashnin, Machine learning-driven synthesis of  $Ti_2ZrNbHfTaC_5$  high-entropy carbide, *npj Comput. Mater.* 9 (2023) 7, <https://doi.org/10.1038/s41524-022-00955-9>.

[19] S. Guan, H. Liang, Q. Wang, L. Tan, F. Peng, Synthesis and phase stability of the high-entropy carbide ( $Ti_{0.2}Zr_{0.2}Nb_{0.2}Ta_{0.2}Mo_{0.2}$ ) under extreme conditions, *Inorg. Chem.* 60 (2021) 3807–3813, <https://doi.org/10.1021/acs.inorgchem.0c03319>.

[20] S. Kavak, K.G. Bayrak, M. Bellek, S. Mertdinç, F. Muhaffel, H. Gökc  , E. Ayas, B. Derin, M.L.   veo  gl  , D. A  ao  ullari, Synthesis and characterization of ( $Hf_0.5Ti_0.5W_0.5$ )C high-entropy carbide ceramics, *Ceram. Int.* 48 (2022) 7695–7705, <https://doi.org/10.1016/j.ceramint.2021.11.317>.

[21] A. Bao, J. Wu, Y. Zhang, X. Wang, X. Zhang, Y. Gu, X. Qi, Facile synthesis of metal carbides with high-entropy strategy for engineering electrical properties, *J. Mater. Res. Technol.* 23 (2023) 1312–1320, <https://doi.org/10.1016/j.jmrt.2023.01.053>.

[22] A. Salian, P. Sengupta, I. Vishalakshi Aswath, A. Gowda, S. Mandal, A review on high entropy silicides and silicates: fundamental aspects, synthesis, properties, *Int. J. Appl. Ceram. Technol.* 20 (2023) 2635–2660, <https://doi.org/10.1111/ijac.14422>.

[23] B. Liu, W. Yang, G. Xiao, Q. Zhu, S. Song, G.-H. Cao, Z. Ren, High-entropy silicide superconductors with  $\langle mth \rangle \langle mrow \rangle \langle msup \rangle \langle mi \mathvariant="normal" \rangle W \langle /mi \rangle \langle mn \rangle 5 \langle /mn \rangle \langle msup \rangle \langle msub \rangle \langle mi \rangle Si \langle /mi \rangle \langle mn \rangle 3 \langle /mn \rangle \langle msup \rangle \langle /mrow \rangle \langle /math \rangle$  – type structure, *Phys. Rev. Mater.* 7 (2023) 014805, <https://doi.org/10.1103/PhysRevMaterials.7.014805>.

[24] C. Chiu, A. Hou, C. Wang, C. Wang, J. Chen, C. Huang, S.H. Chen, Y. Chu, W. Wu, In situ transmission electron microscopy investigation of novel high-entropy silicide ( $Cr_2FeCoNi$ )Si formation at atomic scale, *Small Struct.* (2025), <https://doi.org/10.1002/sstr.202400589>.

[25] Z. Zhang, H. Yi, M. Liang, L. Xie, B. Wang, J. Gao, T. Ma, B. Yin, Y. Yang, Revealing the oxidation and self-healing properties of the in-situ synthesised high-entropy silicide composite ceramics, *Ceram. Int.* (2025), <https://doi.org/10.1016/j.ceramint.2025.02.295>.

[26] L. Lin, K. Wang, A. Sarkar, C. Njel, G. Karkera, Q. Wang, R. Azmi, M. Fichtner, H. Hahn, S. Schweidler, B. Breitung, High-entropy sulfides as electrode materials for Li-ion batteries, *Adv. Energy Mater.* 12 (2022), <https://doi.org/10.1002/aenm.202103090>.

[27] Y. Zhao, J. You, Z. Wang, G. Liu, X. Huang, M. Duan, H. Zhang, High-entropy FeCoNiCuAlV sulfide as an efficient and reliable electrocatalyst for oxygen evolution reaction, *Int. J. Hydrog. Energy* 70 (2024) 599–605, <https://doi.org/10.1016/j.ijhydene.2024.05.186>.

[28] J. Shi, H. Jiang, X. Hong, J. Tang, Non-noble metal high entropy sulfides for efficient oxygen evolution reaction catalysis, *Appl. Surf. Sci.* 642 (2024) 158598, <https://doi.org/10.1016/j.apsusc.2023.158598>.

[29] Y. Pei, D. Li, C. Qiu, L. Yan, Z. Li, Y. Wu, F. Wang, Y. Lu, B. Zhang, High-entropy sulfide catalyst boosts energy-saving electrochemical sulfon upgrading to thiosulfate coupled with hydrogen production, *Angew. Chem.* 136 (2024), <https://doi.org/10.1002/ange.202411977>.

[30] X. Wang, Z. Zhan, H. Cao, Y. Zhang, Preparation of high-entropy nitride composites with fine grain size and high relative density, *Ceram. Int.* 50 (2024) 14948–14958, <https://doi.org/10.1016/j.ceramint.2024.01.409>.

[31] Q. Zhou, F. Xu, C. Gao, W. Zhao, L. Shu, X. Shi, M.-F. Yuen, D. Zuo, Design of high-performance high-entropy nitride ceramics via machine learning-driven strategy, *Ceram. Int.* 49 (2023) 25964–25979, <https://doi.org/10.1016/j.ceramint.2023.05.147>.

[32] V. Novikov, N. Stepanov, S. Zherebtsov, G. Salishchev, Structure and properties of high-entropy nitride coatings, *Metals (Basel)* 12 (2022) 847, <https://doi.org/10.3390/met12050847>.

[33] J. Li, Y. Chen, Y. Zhao, X. Shi, S. Wang, S. Zhang, Super-hard ( $MoSi_2TiV_2Zr$ )<sub>Nx</sub> high-entropy nitride coatings, *J. Alloys Compd.* 926 (2022) 166807, <https://doi.org/10.1016/j.jallcom.2022.166807>.

[34] Z. Wang, Z.-T. Li, S.-J. Zhao, Z.-G. Wu, High-entropy carbide ceramics: a perspective review, *Tungsten* 3 (2021) 131–142, <https://doi.org/10.1007/s42864-021-00085-7>.

[35] Z. Cao, J. Sun, L. Meng, K. Zhang, J. Zhao, Z. Huang, X. Yun, Progress in densification and toughening of high entropy carbide ceramics, *J. Mater. Sci. Technol.* 161 (2023) 10–43, <https://doi.org/10.1016/j.jmst.2023.03.034>.

[36] X. Jin, C. Hou, Y. Zhao, Z. Wang, J. Wang, X. Fan, Mechanical properties and deformation mechanisms of ( $Ti_{0.2}Zr_{0.2}Nb_{0.2}Hf_{0.2}Ta_{0.2}$ )C high-entropy ceramics characterized by nanoindentation and scratch tests, *Ceram. Int.* 48 (2022) 35445–35451, <https://doi.org/10.1016/j.ceramint.2022.08.147>.

[37] S. Yudin, S. Volodko, D. Moskovskikh, I. Alimov, A. Guryanov, S. Zhevnenko, H. Guo, A. Korotitsky, K. Sidnov, S. Roslyakov, C. Zhang, Fabrication of high-entropy carbide ceramics ( $Ti_{1-x}Zr_xNb_xTa_x$ ) through low-temperature calcium-hydride reduction of oxides, *J. Eur. Ceram. Soc.* 43 (2023) 5108–5116, <https://doi.org/10.1016/j.jeurceramsoc.2023.04.056>.

[38] V. Braic, M. Balaceanu, M. Braic, A. Vladescu, S. Panzeri, A. Russo, Characterization of multi-principal-element ( $Ti_{1-x}Zr_xNb_xHf_xTa_x$ )N and ( $Ti_{1-x}Zr_xNb_xHf_xTa_x$ C) coatings for biomedical applications, *J. Mech. Behav. Biomed. Mater.* 10 (2012) 197–205, <https://doi.org/10.1016/j.jmbbm.2012.02.020>.

[39] M. Dinu, I. Pana, A.C. Parau, A. Vlădescu, Tribological Performance of Coatings Obtained by PVD Techniques, 2022, pp. 196–217, <https://doi.org/10.4018/978-1-7998-9683-8.ch009>.

[40] S. Yi, W. Lu, X. Du, Z. Zhang, C. Wu, D. Zuo, High-temperature tribological properties of ( $Ti_{2-x}Nb_xMo_xTa_x$ )N and ( $Ti_{2-x}Nb_xMo_xTa_x$ )CN ceramic coatings, *Wear* 552–553 (2024) 205434, <https://doi.org/10.1016/j.wear.2024.205434>.

[41] S. Yudin, S. Volodko, D. Moskovskikh, I. Alimov, A. Guryanov, S. Zhevnenko, H. Guo, A. Korotitsky, K. Sidnov, S. Roslyakov, C. Zhang, Fabrication of high-entropy carbide ceramics ( $Ti_{1-x}Zr_xNb_xTa_x$ ) through low-temperature calcium-hydride reduction of oxides, *J. Eur. Ceram. Soc.* 43 (2023) 5108–5116, <https://doi.org/10.1016/j.jeurceramsoc.2023.04.056>.

[42] J. Dusza, T. Csan  di, D. Medved, R. Sedl  k, M. Vojtko, M. Ivor, H.   nsal, P. Tatarko, M. Tatarkov  , P.   ajgalik, Nanoindentation and tribology of a ( $Hf-Ta-Zr-Nb-Ti$ )C high-entropy carbide, *J. Eur. Ceram. Soc.* 41 (2021) 5417–5426, <https://doi.org/10.1016/j.jeurceramsoc.2021.05.002>.

[43] L.   akov  , M. Hrubov  ckov  , A. Kovalc  kov  , D. Medved, J. Andrejovsk  , F. Kromka, L. Medveck  , J. Dusza, Influence of sintering condition on tribological properties of ( $Hf-Ta-Zr-Nb-Ti$ )C carbides, *Int. J. Refract. Met. Hard Mater.* 119 (2024) 106549, <https://doi.org/10.1016/j.ijrmhm.2023.106549>.

[44] D. Vedel, T. Csan  di, P. Mazur, A. Osipov, J. Szab  , V. Shvyaniuk, R. Sedl  k, O. Stasiuk, V. Kucharov  , O. Grigoriev, Effect of densification technology on the microstructure and mechanical properties of high-entropy ( $Ti, Zr, Hf, Nb, Ta$ )C ceramic-based cermets, *Open Ceram.* 19 (2024) 100623, <https://doi.org/10.1016/j.oceram.2024.100623>.

[45] P. Istomin, E. Istomina, A. Nadutkin, V. Grass, A. Lysenkov, A. Kudryavtsev, Preparation of ( $Ti_{1-x}Zr_xNb_xTa_x$ )C high-entropy carbide ceramics through carbo-silico-thermic reduction of oxides, *J. Eur. Ceram. Soc.* 41 (2021) 6934–6942, <https://doi.org/10.1016/j.jeurceramsoc.2021.07.012>.

[46] M. Hrubov  ckov  , T. Csan  di, R. Sedl  k, A. Kovalc  kov  , I. Shepa, E. M  dra, T. Sop  c  k, H.   nsal, P. Tatarko, P.   ajgalik, J. Dusza, The effect of SiC whiskers addition on the microstructure and mechanical properties of a ( $Hf-Ta-Zr-Nb-Ti$ )C-SiC composite, *Ceram. Int.* 49 (2023) 24179–24186, <https://doi.org/10.1016/j.ceramint.2022.10.239>.

[47] L. Guo, S. Huang, W. Li, J. Lv, J. Sun, Theoretical design and experimental verification of high-entropy carbide ablative resistant coating, *Adv. Powd. Mater.* 3 (2024) 100213, <https://doi.org/10.1016/j.apmat.2024.100213>.

[48] Y. Wang, Processing and properties of high entropy carbides, *Adv. Appl. Ceram.* 121 (2022) 57–78, <https://doi.org/10.1080/17436753.2021.104277>.

[49] W. Sun, Y. Yang, Y. Wang, High entropy carbide ( $ZrNbTiCr$ )C ceramic composite coating with fine grains fabricated by plasma spraying, *Surf. Coat. Technol.* 478 (2024) 130459, <https://doi.org/10.1016/j.surcoat.2024.130459>.

[50] P. Patel, A. Roy, N. Sharifi, P. Stoyanov, R.R. Chromik, C. Moreau, Tribological performance of high-entropy coatings (HECs): a review, *Materials* 15 (2022) 3699, <https://doi.org/10.3390/ma15103699>.

[51] M. Yin, W. Liang, Q. Miao, H. Yu, W. Yao, K. Zang, Y. Sun, Y. Ma, Y. Wu, X. Gao, Y. Song, Microstructure, mechanical and tribological behavior of  $CrHfNbTaTiCxNy$  high-entropy carbonitride coatings prepared by double glow plasma alloy, *Wear* 523 (2023) 204751, <https://doi.org/10.1016/j.wear.2023.204751>.

[52] X. Lu, L. Yang, Y. Lu, X. Zhang, Z. Yan, J. Hao, W. Liu, Nanostructure, mechanical properties and tribological behavior of high-entropy carbonitrides coatings, *Ceram. Int.* 51 (2025) 13420–13429, <https://doi.org/10.1016/j.ceramint.2025.01.186>.

[53] S. Yi, W. Lu, C. Gao, Z. Zhang, J. Pan, D. Zhao, X. Du, L. Wang, D. Zuo, Composition, structure, and wear resistance of ( $Ti_{2-x}Nb_xMo_xTa_x$ )C N1–high entropy alloy carbonitride coatings prepared by reactive radio-frequency magnetron sputtering, *Surf. Coat. Technol.* 477 (2024) 130333, <https://doi.org/10.1016/j.surcoat.2023.130333>.

[54] Z. Lv, H. Jin, F. Zhang, R. Zhao, S. He, F. Yin, Super-hard yet tough and self-lubricating ( $Ti_{2-x}Nb_xMo_xTa_x$ )C/N high entropy carbonitride films deposited by magnetron sputtering, *Surf. Coat. Technol.* 510 (2025) 132241, <https://doi.org/10.1016/j.surcoat.2025.132241>.

[55] W.H. Kao, Y.L. Su, J.H. Horng, W.C. Wu, Mechanical, tribological, anti-corrosion and anti-glass sticking properties of high-entropy  $TaNbSiZrCr$  carbide coatings prepared using radio-frequency magnetron sputtering, *Mater. Chem. Phys.* 268 (2021) 124741, <https://doi.org/10.1016/j.matchemphys.2021.124741>.

[56] T. Stasiak, S. Debn  rov  , S. Lin, N. Koutn  , Z. Czig  ny, K. Bal  zsi, V. Bur  sikov  , P. Vasina, P. Sou  ek, Synthesis and characterization of ceramic high-entropy carbide thin films from the Cr-Hf-Mo-Ta-W refractory metal system, *Surf. Coat. Technol.* 485 (2024) 130839, <https://doi.org/10.1016/j.surcoat.2024.130839>.

[57] C. Li, G. Li, W. L  , J. Deng, Z. Song, Q. Wang, Effect of carbon content on the structure and mechanical properties of ( $TiAlTaCrZr$ )CN high entropy alloy carbonitride coatings prepared by magnetron sputtering, *Ceram. Int.* 51 (2025) 11499–11508, <https://doi.org/10.1016/j.ceramint.2025.01.004>.

- [58] T. Wang, C. Wang, J. Li, W. Wang, L. Chai, J. Luo, Oxidation resistance, corrosion behavior and grinding performance of laser-deposited TaMoCrTiAl refractory high-entropy coating, Int. J. Refract. Met. Hard Mater. 123 (2024) 106771, <https://doi.org/10.1016/j.ijrmhm.2024.106771>.
- [59] P. Patel, R.B. Nair, R. Supekar, A. McDonald, R.R. Chromik, C. Moreau, P. Stoyanov, Enhanced wear resistance of AlCoCrFeMo high entropy coatings (HECs) through various thermal spray techniques, Surf. Coat. Technol. 477 (2024) 130311, <https://doi.org/10.1016/j.surcoat.2023.130311>.
- [60] W. Sun, Y. Yang, Y. Wang, High entropy carbide (ZrNbTiCr)C ceramic composite coating with fine grains fabricated by plasma spraying, Surf. Coat. Technol. 478 (2024) 130459, <https://doi.org/10.1016/j.surcoat.2024.130459>.
- [61] I. Shanankov, D. Nikitin, A. Ivashutenko, I. Rahmatullin, Y. Shanankova, A. Nasyrbayev, W. Han, A. Sivkov, Hardening the surface of metals with WC<sub>1-x</sub> coatings deposited by high-speed plasma spraying, Surf. Coat. Technol. 389 (2020) 125639, <https://doi.org/10.1016/j.surcoat.2020.125639>.
- [62] A.G. Kvashnin, D.S. Nikitin, I.I. Shanankov, I.V. Chepkasov, Y.A. Kvashnina, A. Nasyrbayev, A.A. Sivkov, Z. Bolatova, A.Y. Pak, Large-scale synthesis and applications of hafnium–tantalum carbides, Adv. Funct. Mater. (2022), <https://doi.org/10.1002/adfm.202206289>.
- [63] J.W. Yeh, S.K. Chen, S.J. Lin, J.Y. Gan, T.S. Chin, T.T. Shun, C.H. Tsau, S.Y. Chang, Nanostructured high-entropy alloys with multiple principal elements: novel alloy design concepts and outcomes, Adv. Eng. Mater. 6 (2004) 299–303, <https://doi.org/10.1002/ADEM.200300567>.
- [64] S.V. Bobashev, B.G. Zhukov, R.A. Kurakin, S.A. Ponyaev, B.I. Reznikov, S.I. Rozov, Parameters of an erosive carbon plasma in the channel of a railgun, Tech. Phys. 55 (2010) 1754–1759, <https://doi.org/10.1134/S1063784210120078/METRICS>.
- [65] I. Shanankov, D. Nikitin, A. Ivashutenko, I. Rahmatullin, Y. Shanankova, A. Nasyrbayev, W. Han, A. Sivkov, Hardening the surface of metals with WC<sub>1-x</sub> coatings deposited by high-speed plasma spraying, Surf. Coat. Technol. 389 (2020) 125639, <https://doi.org/10.1016/j.surcoat.2020.125639>.
- [66] A.A. Sivkov, D.S. Nikitin, A.Ya. Pak, I.A. Rakhmatullin, Influence of plasmodynamic synthesis energy in Si-C system on the product phase composition and dispersion, Nanotechnol. Russ. 10 (2015) 34–41, <https://doi.org/10.1134/S1995078015010188>.
- [67] A. Bao, J. Wu, Y. Zhang, X. Wang, X. Zhang, Y. Gu, X. Qi, Facile synthesis of metal carbides with high-entropy strategy for engineering electrical properties, J. Mater. Res. Technol. 23 (2023) 1312–1320, <https://doi.org/10.1016/J.JMRT.2023.01.053>.
- [68] P. Hohenberg, W. Kohn, Inhomogeneous electron gas, Phys. Rev. 136 (1964) B864–B871, <https://doi.org/10.1103/PhysRev.136.B864>.
- [69] W. Kohn, L.J. Sham, Self-consistent equations including exchange and correlation effects, Phys. Rev. 140 (1965) A1133–A1138, <https://doi.org/10.1103/PhysRev.140.A1133>.
- [70] J.P. Perdew, K. Burke, M. Ernzerhof, Generalized gradient approximation made simple, Phys. Rev. Lett. 77 (1996) 3865–3868, <https://doi.org/10.1103/PhysRevLett.77.3865>.
- [71] P.E. Blöchl, Projector augmented-wave method, Phys. Rev. B 50 (1994) 17953–17979, <https://doi.org/10.1103/PhysRevB.50.17953>.
- [72] G. Kresse, D. Joubert, From ultrasoft pseudopotentials to the projector augmented-wave method, Phys. Rev. B 59 (1999) 1758–1775, <https://doi.org/10.1103/PhysRevB.59.1758>.
- [73] G. Kresse, J. Hafner, *Ab initio* molecular dynamics for liquid metals, Phys. Rev. B 47 (1993) 558–561, <https://doi.org/10.1103/PhysRevB.47.558>.
- [74] G. Kresse, J. Hafner, *Ab initio* molecular-dynamics simulation of the liquid-metal-amorphous-semiconductor transition in germanium, Phys. Rev. B 49 (1994) 14251–14269, <https://doi.org/10.1103/PhysRevB.49.14251>.
- [75] G. Kresse, J. Furthmüller, Efficient iterative schemes for *ab initio* total-energy calculations using a plane-wave basis set, Phys. Rev. B 54 (1996) 11169–11186, <https://doi.org/10.1103/PhysRevB.54.11169>.
- [76] M. Methfessel, A.T. Paxton, High-precision sampling for Brillouin-zone integration in metals, Phys. Rev. B 40 (1989) 3616–3621, <https://doi.org/10.1103/PhysRevB.40.3616>.
- [77] B. Schuh, B. Völker, J. Todt, N. Schell, L. Perrière, J. Li, J.P. Couzinié, A. Hohenwarter, Thermodynamic instability of a nanocrystalline, single-phase TiZrNbHfTa alloy and its impact on the mechanical properties, Acta Mater. 142 (2018) 201–212, <https://doi.org/10.1016/J.ACTAMAT.2017.09.035>.
- [78] S.Y. Chen, Y. Tong, K.K. Tseng, J.W. Yeh, J.D. Poplawsky, J.G. Wen, M.C. Gao, G. Kim, W. Chen, Y. Ren, R. Feng, W.D. Li, P.K. Liaw, Phase transformations of HfNbTaTiZr high-entropy alloy at intermediate temperatures, Scr. Mater. 158 (2019) 50–56, <https://doi.org/10.1016/J.SCRIPTAMAT.2018.08.032>.
- [79] M.J. Liu, M. Zhang, X.F. Zhang, G.R. Li, Q. Zhang, C.X. Li, C.J. Li, G.J. Yang, Transport and deposition behaviors of vapor coating materials in plasma spray-physical vapor deposition, Appl. Surf. Sci. 486 (2019) 80–92, <https://doi.org/10.1016/j.apsusc.2019.04.224>.
- [80] X. Zhang, C. Wang, R. Ye, C. Deng, X. Liang, Z. Deng, S. Niu, J. Song, G. Liu, M. Liu, K. Zhou, J. Lu, J. Feng, Mechanism of vertical crack formation in Yb<sub>2</sub>SiO<sub>5</sub> coatings deposited via plasma spray-physical vapor deposition, J. Mater. 6 (2020) 102–108, <https://doi.org/10.1016/j.jmat.2020.01.002>.
- [81] O.F. Dippo, N. Mesgarzadeh, T.J. Harrington, G.D. Schrader, K.S. Vecchio, Bulk high-entropy nitrides and carbonitrides, Sci. Rep. 10 (2020) 1–11, <https://doi.org/10.1038/s41598-020-78175-8>.
- [82] T. Wen, B. Ye, M.C. Nguyen, M. Ma, Y. Chu, Thermophysical and mechanical properties of novel high-entropy metal nitride-carbides, J. Am. Ceram. Soc. 103 (2020) 6475–6489, <https://doi.org/10.1111/JACE.17333>.
- [83] D. Moskovskikh, S. Vorotilo, V. Buinevich, A. Sedegov, K. Kuskov, A. Khort, C. Shuck, M. Zhukovskiy, A. Mukasyan, Extremely hard and tough high entropy nitride ceramics, Sci. Rep. 10 (2020) 1–8, <https://doi.org/10.1038/s41598-020-76945-y>.
- [84] P. Sarker, T. Harrington, C. Toher, C. Oses, M. Samiee, J.-P. Maria, D.W. Brenner, K.S. Vecchio, S. Curtarolo, High-entropy high-hardness metal carbides discovered by entropy descriptors, Nat. Commun. 9 (2018) 4980, <https://doi.org/10.1038/s41467-018-07160-7>.
- [85] X.-Q. Chen, H. Niu, D. Li, Y. Li, Modeling hardness of polycrystalline materials and bulk metallic glasses, Intermetallics (Barking) 19 (2011) 1275–1281, <https://doi.org/10.1016/j.intermet.2011.03.026>.
- [86] E. Mazhnik, A.R. Oganov, A model of hardness and fracture toughness of solids, J. Appl. Phys. 126 (2019), <https://doi.org/10.1063/1.5113622>.
- [87] Q. Yang, W. Lengauer, T. Koch, M. Scheerer, I. Smid, Hardness and elastic properties of Ti(CxN<sub>1-x</sub>), Zr(CxN<sub>1-x</sub>) and Hf(CxN<sub>1-x</sub>), J. Alloys Compd. 309 (2000) L5–L9, [https://doi.org/10.1016/S0925-8388\(00\)01057-4](https://doi.org/10.1016/S0925-8388(00)01057-4).
- [88] K. Balasubramanian, S.V. Khare, D. Gall, Valence electron concentration as an indicator for mechanical properties in rocksalt structure nitrides, carbides and carbonitrides, Acta Mater. 152 (2018) 175–185, <https://doi.org/10.1016/j.actamat.2018.04.033>.
- [89] O.F. Dippo, N. Mesgarzadeh, T.J. Harrington, G.D. Schrader, K.S. Vecchio, Bulk high-entropy nitrides and carbonitrides, Sci. Rep. 10 (2020) 21288, <https://doi.org/10.1038/s41598-020-78175-8>.
- [90] C. Wiemer, R. Sanjinés, F. Lévy, Deposition and characterization of refractory ternary phases: the transition metal nitride Ti<sub>1-x</sub>M<sub>x</sub>Ny, Surf. Coat. Technol. 86–87 (1996) 372–376, [https://doi.org/10.1016/S0257-8972\(96\)02953-2](https://doi.org/10.1016/S0257-8972(96)02953-2).
- [91] D.G. Sangiovanni, L. Hultman, V. Chirita, Supertoughening in B1 transition metal nitride alloys by increased valence electron concentration, Acta Mater. 59 (2011) 2121–2134, <https://doi.org/10.1016/j.actamat.2010.12.013>.
- [92] T. Wen, B. Ye, M.C. Nguyen, M. Ma, Y. Chu, Thermophysical and mechanical properties of novel high-entropy metal nitride-carbides, J. Am. Ceram. Soc. 103 (2020) 6475–6489, <https://doi.org/10.1111/JACE.17333>.
- [93] A.G. Kvashnin, Z. Allahyari, A.R. Oganov, Computational discovery of hard and superhard materials, J. Appl. Phys. 126 (2019), <https://doi.org/10.1063/1.5109782>.
- [94] T.T. Nguyen, M. Arita, R. Saeki, K. Edalati, High-entropy oxide Ti-Zr-Hf-Nb-Ta-O as photoanode for photoelectrocatalytic hydrogen generation, Scr. Mater. 264 (2025) 116698, <https://doi.org/10.1016/J.SCRIPTAMAT.2025.116698>.
- [95] P. Edalati, Q. Wang, H. Razavi-Khosroshahi, M. Fuji, T. Ishihara, K. Edalati, Photocatalytic hydrogen evolution on a high-entropy oxide, J. Mater. Chem. A Mater. 8 (2020) 3814–3821, <https://doi.org/10.1039/C9TA12846H>.